RESPONSE OF SEISMICALLY ISOLATED CYLINDRICAL LATTICED SHELL WITH HDR UNDER SPATIALLY VARYING EARTHQUAKE GROUND MOTIONS

MINGYUE SHAN[1,2], SHAODONG SHEN[1], PENG PAN[1,*]

[1]*Department of Civil Engineering, Tsinghua University, Qinghuayuan, Haidian District, Beijing, China*
** E-mail: panpeng@tsinghua.edu.cn*

[2]*Spatial Structures Research Center, Beijing University of Technology, No. 100, Pingleyuan, Chaoyang District, Beijing, China*

The influences on structural response of large span latticed shell with HDR bearings were investigated based on spatial variation of earthquake ground motion. Serial numerical simulations of a column supported single-layer cylindrical latticed shell with high-position seismically isolation by HDR bearings under uniform excitation and multi-support excitation were carried out. A numerical model for the support columns-HDR bearings-large span cylindrical latticed shell was presented, in which the damping matrix was formed by the Clough non-proportional damping theory. The three-dimensional Timoshenko beam element was applied to represent the restoring-force characteristics of HDR bearing. The results showed that the HDR bearings prolonged the natural vibration period of the cylindrical latticed shell and the structural deformation induced by earthquake ground motion mainly occurred at the HDR bearing locations. The cylindrical latticed shell roof exhibited a consistently paced movement and the difference between the inner forces at various parts of the structure decreased. The high-position seismically isolation with the HDR bearings reduced the peak acceleration of horizontal earthquake response notably. Considering the wave-passage effect, the cylindrical latticed shell structural responses decreased at wave inlet and notably increased at wave outlet.

Keywords: High damping rubber bearing (HDR), seismic isolation, cylindrical latticed shell, multi-support excitations.

1 Introduction

The latticed shell is a spatially curved truss or beam structure composed of special patterned member bars and connecting joints. Given the randomness and complexity of earthquakes, it is difficult for a traditional aseismic design to meet the structural safety requirements. Therefore, the seismic isolation design has become an effective technique. In the terminal structure of Kunming Changshui International Airport, China (Lu *et al*., 2011), which exhibits a double-layer hyperbolic paraboloid latticed shell, a composite seismic isolation design with lead rubber bearings, normal rubber bearings, and viscoelastic dampers was applied and the efficiency has thus been proved notable. The recently completed Beijing Daxing Airport, China, (Shu *et al*., 2016) adopting interlayer seismic isolation technology, which contains a total number of seismic isolations and hysteretic dampers of 1118.

The spatial variability effect of ground motion notably influences the earthquake response of structures with large spans and lengths. Zanardo et al. (2002) performed a parametrical study

Proceedings of the 17th International Symposium on Tubular Structures.
Editors: X.D. Qian and Y.S. Choo

Published by Research Publishing, Singapore.
ISBN: 978-981-11-0745-0; doi:10.3850/978-981-11-0745-0_054-cd

of pounding phenomenon associated with the seismic response of multi-span simply supported bridges with base isolation bearings, wherein a three-dimensional finite element model was defined. The numerical results suggested that pounding forces by a spatially varying input could values 3 to 4-fold larger than those obtained by analysis with uniform input. Xue et al. (2004) studied the non-stationary random response of a double-layer cylindrical latticed shell under multiple dimensional and multiple support inputted by applying pseudo-excitation method and suggested a method for estimating the peak values of structural responses. Shu et al. (2009) performed a time history analysis on the terminal hall of the Kunming Changshui International Airport under multiple support and multiple dimensional input. The results evidenced the adoption of base isolations would made the torsion of the upper multilayer structure caused by wave-passage excitation more consistent and also mitigates the wave-passage effect.

The damping ratio of the HDR bearing is known to be much higher than that of steel, which leads to a damping concentration at the isolation bearing sites and results in an uneven damping distribution within the overall system. In this paper, the damping matrix of the entire structure system is formed by non-proportional damping theory. The seismic performance of single-layer cylindrical latticed shell with HDR is studied taking the influence of wave-passage effect into account.

2 Equation of seismically isolated latticed shell under multi-support excitation

2.1 *Theoretical model of cylindrical latticed shell with HDR bearings*

The damping ratio of HDR can reach a value of 0.15 following improvements in the rubber formula. The horizontal rigidity coefficient is computed as:

$$K_{\mathrm{h}} = G_{\mathrm{eq}}(\gamma)\frac{A}{T_{\mathrm{r}}} \tag{1}$$

where $G_{\mathrm{eq}}(\gamma)$ is the equivalent shear modulus at shear strain γ; G is constant while ignoring the shear strain influence on shear modulus of rubber; A is the cross-sectional area of HDR; T_{r} is the total thickness of the rubber.

The equivalent damping ratio h_{eq} is computed by Eq. (2):

$$h_{\mathrm{eq}} = \frac{1}{2\pi}\frac{W_{\mathrm{d}}}{K_{\mathrm{h}}X^2} \tag{2}$$

where W_{d} is the area encircled by the shear force-shear displacement hysteresis loop; K_{h} is the horizontal equivalent stiffness of HDR; and X is the shear displacement.

The three-dimensional Timoshenko beam element is applied to represent the mechanical property of the HDR bearing, with the deflection w and rotational angle θ interpolated independently. Each element contains two nodes. In local coordinate system, the element rigidity matrix is represented as:

$$\boldsymbol{K}^{\mathrm{e}} = \begin{bmatrix} \boldsymbol{k}_{11} & \boldsymbol{k}_{12} \\ \boldsymbol{k}_{12}^{\mathrm{T}} & \boldsymbol{k}_{22} \end{bmatrix} \tag{3}$$

Because of the rotational angle θ of the Timoshenko beam element has nothing to do with the deflection w, assume $\theta = 0$ and $dw/dx = \gamma$, all the rotation terms in the rigidity matrix were set to zero such that the shear strain along the height of the HDR bearing was constant (Fig.1).

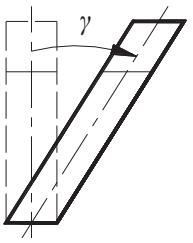

Fig.1 The constant shear strain of the Timoshenko beam element

The natural vibration frequencies of seismically isolated cylindrical latticed shell without damping are calculated using the subspace iteration method. Because the impact of damping on structural frequencies is limited, it is acceptable to replace the actual values with these results. Since the shear stiffness of rubber bearings is relatively less than stiffness of the structural members, the deformations excited by earthquake mainly occur at the isolation bearing sites, thus leading to decrease of mode numbers that have greater contribution to structural deformations. Therefore, only the natural vibration frequencies of the first two modes ω_1 and ω_2 are adopted and the damping matrix of the latticed shell with HDR bearings is established as follows:

The Rayleigh damping coefficients a_0 and a_1 are given using a damping ratio $\xi = \xi_1 = \xi_2 = 0.02$ for the whole structure (without the damping of the HDR bearings), thus the damping matrix is represented as:

$$\boldsymbol{C} = a_0 \boldsymbol{M} + a_1 \boldsymbol{K} \tag{4}$$

Assumes the damping ratio ξ_r of the HDR bearing was 0.15. By subtracting the damping ratio set for the corresponding position of HDR bearings in the structure of 0.02, the actual damping ratio for the bearings ξ_r'=0.13. Calculating the Rayleigh damping coefficients a_{0r} and a_{1r}, the element damping matrix of each HDR bearing can be represented as:

$$\boldsymbol{C}_{ri} = a_{0r} \boldsymbol{M}_{ri} + a_{1r} \boldsymbol{K}_{ri} \tag{5}$$

The element damping matric C_{ri} of each HDR bearing is integrated into the global damping matrix C_r using position vectors. The global damping matrix of the seismically isolated cylindrical latticed shell can be represented as:

$$\overline{\boldsymbol{C}} = \boldsymbol{C} + \boldsymbol{C}_r \tag{6}$$

Introducing the global non-proportional damping matrix $\overline{\boldsymbol{C}}$ into governing equation of Large Mass Method (Liu ,2015).

2.2 *Spatially varying earthquake ground motion model*

Earthquake waves travel at speeds of 800–2500 m/s in bedrock, while at 150–250 m/s in soft soils. Therefore, the finite propagating velocity of earthquake waves results in different arrival times at various ground points, such in the case of delays in arrival times for column bottoms of the cylindrical latticed shell.

3 Numerical example

3.1 *Structural model*

A numerical model was presented for a single-layer cylindrical latticed shell supported by surrounding columns. The upper cylindrical latticed shell was designed to follow the general three-way grid with a total length of L = 200 m, a column space of 40 m, a width of B = 20 m, and an arch height of 3 m. In the structural design, the constant load of the profiled steel sheet and purlin bracing was estimated to be 0.45 kN/m^2. Its two lengthwise sides were supported by 12 independent steel columns. The layout of the cylindrical latticed shell model is presented in Fig.2.

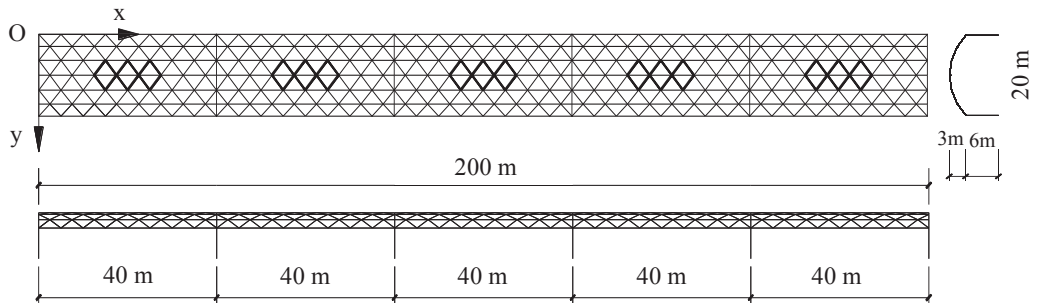

Fig.2 Analytical model of the cylindrical latticed shell structure

The cross section of the member bars along x-axis edges is Φ325×16. The lateral bars were set between each pair of columns along the y-axis to reinforce lateral stiffness, with cross section as Φ245×14. The cross section of the inner bars (neglecting lateral bars) is Φ165×5 and the cross section of the inner bars (thickened) is Φ180×8. The Young's modulus of steel in this model is 206 GPa. The connections between structural members and structural member-foundations were all supposed to be rigid. The outer diameter of the HDR bearing d_0 is 420 mm and the diameter of centre-hole d is 70 mm. The total thickness of the rubber T is 168 mm, with a material shear modulus G = 0.8 MPa. The damping ratio ξ_r of the HDR bearing is 0.15. The HDR bearings were installed on top of each column.

Model analysis was performed for non-isolated and seismically isolated cylindrical latticed shells using the subspace iteration method. The first four natural vibration frequencies were shown in Table 1. Results showed the cylindrical latticed shell periods have been increased notably with the HDR bearings.

Table 1 Vibration frequencies of the non-isolated and isolated cylindrical latticed shells

Mode No.	Frequency (Hz)		Mode No.	Frequency (Hz)	
	Non-isolated	Isolated		Non-isolated	Isolated
1	1.0401	0.3560	3	1.1604	0.3917
2	1.0796	0.3655	4	1.2482	0.5604

O$_D$ x

D

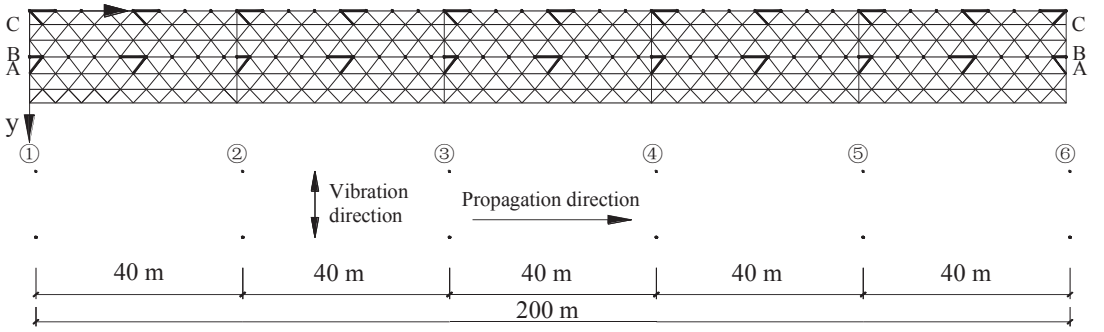

Fig. 3 Sketch for bars and joints being analysis

Several groups of structural members were selected, either with large inner forces or at sample locations, including two columns of joints along the lengthwise direction and four columns of member bars, which were denoted with solid circle points or thick solid lines, coded A, B, C, and D in Fig. 3. The dynamic responses of the structural members at other positions were obtained by symmetry.

3.2 *Analysis for the wave-passage effect in the horizontal direction*

The Pixian Zoushishan wave(E-W) was selected as seismic input along the low stiffness direction (y-axis) of the numerical model. The wave was recorded on May 12, 2008, on bedrock site, Pixian County, Sichuan Province by Chengdu Seismostation. The duration of the Pixian Zoushishan wave is 121.27s and the maximum acceleration is 120.34 cm/s^2. The original record of Pixian Zoushishan wave(E-W) is presented in Fig.4. According to the availability of wave propagation and the actual condition of engineering, dynamic responses under the infinite visual wave velocity, 2000 m/s and 1000 m/s are computed, of which the infinite case is equivalent with uniform excitation. The peak value of the input acceleration is adjusted to 400 cm/s^2.

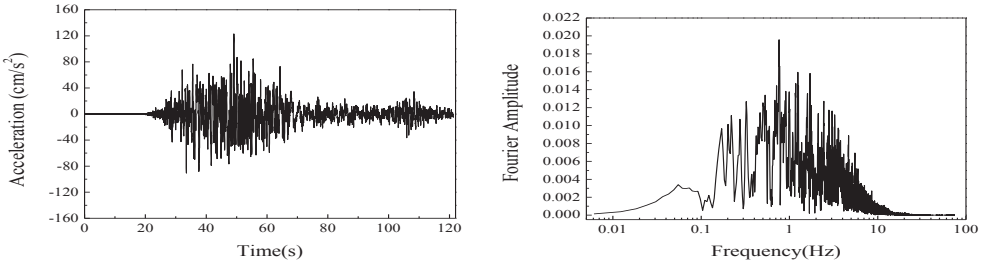

(a) Acceleration time history (b) Fourier amplitude spectrum

Fig.4 Pixian Zoushishan wave of Wenchuan earthquake (EW)

* Means of symbols in Fig.5-Fig.7

—△— non-isolated, uniform excitation —□— seismically isolated, uniform excitation
—▲— non-isolated, 2000m/s —■— seismically isolated, 2000m/s
—◭— non-isolated, 1000m/s —◧— seismically isolated, 1000m/s

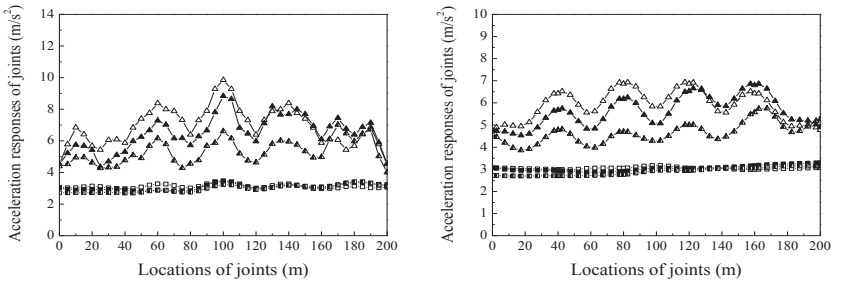

(a) Joints on column D-D (b) Joints on column B-B

Fig.5 Maximum accelerations of joints for Pixian Zoushishan wave (EW; 4 m/s^2)

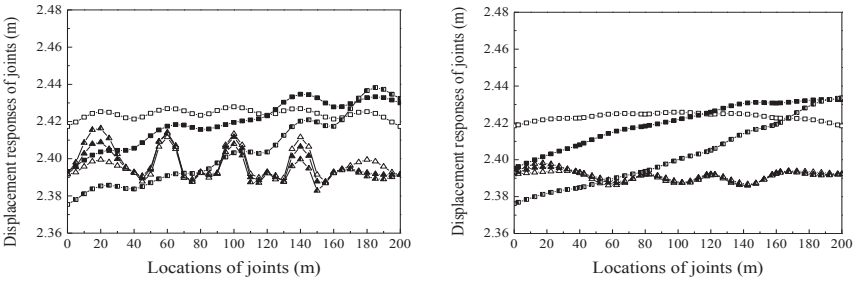

(a) Joints on column D-D (b) Joints on column B-B

Fig.6 Maximum displacements of joints for Pixian Zoushishan wave (EW; 4 m/s^2)

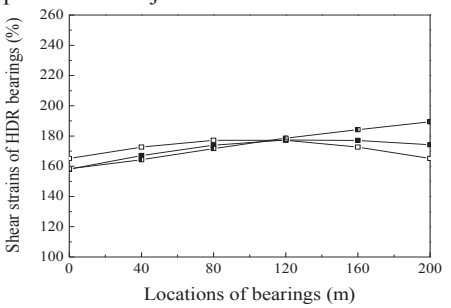

Fig. 7 Maximum shear strains at HDB bearings

Variations in the earthquake response of the cylindrical latticed shell following the installation of the HDR bearings are presented in Figs.5- Figs.7 under uniform excitation and multi-support excitation, respectively.

The maximum acceleration responses for the joints of non-isolated and seismically isolated cylindrical latticed shells under excitation of the Pixian Zoushishan wave in the y-direction are presented in Fig. 5. Figure 5(a) presents the response values of joints on side column D-D at y = 0 m, while Fig. 5(b) presents the joints on lateral mid-span column B-B at y = 10 m. For the non-isolated structure, the maximum accelerations of joints near mid-span (x = 20 m, 60 m, 100 m, 140 m, and 180 m) on column D-D were notably larger than that near the column tops (x = 0 m, 40 m, 80 m, 120 m, 160 m, and 200 m). Specifically, the maximum joint acceleration at x = 100 m exceeded 10 m/s^2, thereby leading to a peak distribution at center and lower portion of two sides. On the contrary, the maximum accelerations of joints near the lateral members (x = 0 m, 40 m, 80 m, 120 m, 160 m, and 200 m) on column B-B were notably larger than that near mid-span. The distribution of the maximum accelerations of joints was symmetrical along the x-axis length due to structural symmetry of the cylindrical latticed shell.

Under wave-passage excitation, the maximum accelerations of joints tended to be enlarged along the direction of earthquake wave propagation from the wave input side to the output side as compared to that of uniform excitation. At the visual wave velocity V_a of 2000 m/s, the maximum accelerations of joints within x = 0–130 m decreased by 11%–20%, whereas joints within x = 130–200 m increased by 9%–24%. At the visual wave velocity V_a of 1000 m/s, the maximum accelerations of joints within x = 0–130 m further decreased, but increased along the wave propagation direction. The non-symmetrical maximum acceleration distribution was significant following the decrease of visual wave velocity.

The shear stiffness of the rubber bearings were significantly less than that of the cylindrical latticed shell; therefore, the adoption of HDR bearings concentrated the earthquake-excited deformations mainly at the bearings, producing single-phase motion predominance in the cylindrical latticed shell. The differences in maximum accelerations between joints were negligible. The peak joint accelerations decreased remarkably and the most notable dropdown occurred at x=100 m of side column D-D, with observed maximum joint acceleration at only 35% without seismic isolation. Adding up the wave-passage effect, the maximum joints accelerations increased along the lengthwise direction. At visual wave velocity V_a of 1000 m/s, the maximum acceleration of joint at the wave output side increased by 10% as compared to uniform excitation, though still less than the case without seismic isolation.

Following the use of HDR bearings, the absolute displacements of joints exhibited a minimal increase as shown in Fig. 6. Under wave-passage excitation, the joint displacements increased along the wave propagation direction, which is similar to the variations of the joint accelerations. Lower visual wave velocity produced smaller displacements at the inlet end but larger outlet displacements compared to uniform excitation.

The shear deflections of HDR bearings under wave-passage excitation are presented in Fig. 7. The maximum shear deflection decreases at the earthquake wave inlet, and increases at outlet by 15% at the visual wave velocity V_a of 1000 m/s.

4 Conclusions

- The HDR bearings prolonged the natural vibration period of the cylindrical latticed shell. The structural deformation induced by earthquake ground motion mainly occurred at the HDR bearings. The cylindrical latticed shell roof exhibited a consistently paced movement and the difference between the inner forces at various parts of the structure decreased. The acceleration responses of joints were only 1/28-1/2 of that without HDR bearings. The HDR bearings exhibited a notable isolation and mitigation efficiency on the cylindrical latticed shell structure.
- Considering the wave-passage effect, the structural responses (joint accelerations, joint displacements, and shear strains of HDR bearings) of the cylindrical latticed shell structure decreased at wave inlet and notably increased at wave outlet. The dynamic responses increased along the wave propagation direction and this tendency was more notable with the decrease of wave visual velocity.

References

Giovanna Zanardo, Hong Hao and Claudio Modena, Seismic response of multi-span simply supported bridges to a spatially varying earthquake ground motion, *Earthquake engineering and structural dynamics*, 31(6), 1325-1345, 2002.

Xue Suduo, Wang Xuesheng and Cao Zi, An efficient algorithm for multi-dimensional and multi-support random seismic analysis of spatial reticulated structures, *World Earthquake Engineering*, 20(3), 43-49, 2004.

Shu Weinong, Li Huafeng, Bu Longgui, et al., Multi-support and multi-dimension excitation seismic analysis on new Kunming Airport building, *Building Structure*, 39(12), 68-70, 2009.

Lu Weidong, Liu Weiqing, Wu Xiaofei, et al., Shaking table test of Terminal A structure of Kunming International Airport, *Journal of Building Structures*, 32(6), 27-33, 2011.

Li Xiongyan, Xue Suduo and Cai Yancheng, Three–dimensional seismic isolation bearing and its application in long span hangars, *Earthquake engineering and engineering vibration*, 12(1), 55-65, 2013.

Liu Guohuan, Guo Wei, *Theory, model and method of spatially variable earthquake motions input for structural analysis*, China Science Publishing & Media Ltd, Beijing, 2015.

Shu Weinong, Zhu Zhongyi, Qi Yue, et al., Design and research on terminal building of Beijing New Airport. *Building Structure*, 46(17), 1-7, 2016.